materials

MDPI

Article

High-throughput Production of ZnO-MoS_2-Graphene Heterostructures for Highly Efficient Photocatalytic Hydrogen Evolution

Haocong Dong [1,2], Junzhu Li [2,3], Mingguang Chen [3], Hongwei Wang [2,4], Xiaochuan Jiang [2,5], Yongguang Xiao [1,*], Bo Tian [2,3,*] and Xixiang Zhang [3,*]

1 Key Laboratory of Film Materials & Application for Equipment, School of Materials Science and Engineering, Xiangtan University, Xiangtan 411105, China
2 Eleven-Dimensional Nanomaterial Research Institute, Xiamen 361000, China
3 Physical Science and Engineering Division, King Abdullah University of Science and Technology (KAUST), Thuwal 23955-6900, Saudi Arabia
4 State Key Laboratory of Advanced Optical Communication Systems and Networks, Department of Electronic Engineering Shanghai Jiao Tong University, Shanghai 200240, China
5 Department of Astronomy, Xiamen University, Xiamen 361000, China
* Correspondence: ygxiao@xtu.edu.cn (Y.X.); bo.tian@kaust.edu.sa (B.T.); xixiang.zhang@kaust.edu.sa (X.Z.)

Received: 30 May 2019; Accepted: 8 July 2019; Published: 11 July 2019

Abstract: High-throughput production of highly efficient photocatalysts for hydrogen evolution remains a considerable challenge for materials scientists. Here, we produced extremely uniform high-quality graphene and molybdenum disulfide (MoS_2) nanoplatelets through the electrochemical-assisted liquid-phase exfoliation, out of which we subsequently fabricated MoS_2/graphene van der Waals heterostructures. Ultimately, zinc oxide (ZnO) nanoparticles were deposited into these two-dimensional heterostructures to produce an artificial ZnO/MoS_2/graphene nanocomposite. This new composite experimentally exhibited an excellent photocatalytic efficiency in hydrogen evolution under the sunlight illumination ($\lambda > 400\ nm$), owing to the extremely high electron mobilities in graphene nanoplatelets and the significant visible-light absorptions of MoS_2. Moreover, due to the synergistic effects in MoS_2 and graphene, the lifetime of excited carriers increased dramatically, which considerably improved the photocatalytic efficiency of the ZnO/MoS_2/graphene heterostructure. We conclude that the novel artificial heterostructure presented here shows great potential for the high-efficient photocatalytic hydrogen generation and the high throughput production of visible-light photocatalysts for industrial applications.

Keywords: graphene; MoS_2; ZnO; photocatalyst; high-throughput production

1. Introduction

Photocatalytic hydrogen-evolution nanotechnologies under visible-light illumination have attracted tremendous and growing interest from the scientific communities due to their significant potential for the storage of solar energy and the production of green energy. In recent decades, various methods and nanostructures have been developed to realize efficient hydrogen generation [1,2]. As examples, a photostable photocatalyst of n-doped zinc oxide (ZnO)/graphene oxide has been developed for improving the mineralization and photodegradation of organic dye under visible light [3–5]; "green" SnS_2 quantum dots/reduced graphene oxide composites have been fabricated with enhanced photocatalytic performance [6]; and Pd-decorated ZnO−graphene oxide nanocomposites have been reported with significantly enhanced photocatalytic activities based on a charge separation mechanism [7]. However, due to the limited lifetime of excited electrons and holes, as well as the poor

abilities of visible-light absorption in ordinary materials, high-efficient mass-produced sunlight-driven photocatalysts remain strongly desired.

Low-dimensional nanomaterials, such as quantum dots and two-dimensional materials, are expected to be the new-generation photocatalytic materials because of their excellent physical and chemical properties. Zinc oxide (ZnO) nanoparticles are emerging as a competitive photocatalyst, due to their outstanding photoelectricity, regulable band gap, and extremely high electron densities [8,9]. However, the rapid recombination of photogenerated electrons and holes in ZnO nanoparticles, as well as the poor capabilities of visible-light absorption deteriorated the ZnO nanoparticles' photocatalytic performances [10–13]. Even though some researchers have managed to combine the ZnO nanoparticles with graphene oxide [14], which served as the electron transport layer, the photocatalytic efficiency was not significantly improved, because it was restricted by the self-aggregation effect of these nanoparticles and the low conductivity of graphene oxide.

Graphene, the 'superstar' of two-dimensional materials with excellent electric, thermal, and mechanical properties [15–17], was used to replace graphene oxide in order to improve the photocatalytic performance of ZnO/graphene oxide heterostructures by reducing the recombination rates of excited electrons and holes in the photocatalytic processes [18–23]. However, ZnO/graphene structures still could not reach a satisfactory catalytic performance, due to the weak absorption capability of visible light. For this reason, we proposed to fabricate a ZnO/MoS_2/graphene heterostructure, in which MoS_2, generally considered to be a layered n-type semiconductor with a suitable band gap for the absorption of visible light, serves as an interlayer to the sunlight absorption and thus improves the photocatalytic efficiency [24–26]. In addition, this two-dimensional MoS_2 also significantly enhances the transportation of excited carriers in the composite, leading to a higher photocatalytic efficiency [27,28].

In this work, we exfoliated graphite into high-quality graphene nanoplatelets in solvents, produced high-quality layered MoS_2 by the electrochemical-assisted liquid-phase exfoliation method [29], and assembled these two-dimensional materials to MoS_2/graphene van der Waals heterostructures [30]. Next, ZnO nanoparticles were chemically synthesized and incorporated into the MoS_2/graphene nanostructures to form ZnO/MoS_2/graphene ternary heterostructures. Relying on the extremely-high carrier mobilities and the large effective surface of graphene nanoplates, as well as the enhanced visible-light absorption of the electron-transport-layered MoS_2 [31–34], these heterostructures no only exhibited the high photocatalytic efficiency in the generation of hydrogen but also reached an efficiency five times higher than that previously reported of graphene-oxide-based photocatalysts. It is worth noting that the new heterostructures were quite easily synthesized, as the preparation process of non-oxidized pure graphene nanoplatelets is faster and more straightforward, owing to the lack of oxidation-reduction process [35]. Our synthetic process also offers the possibility to be performed in large-scale ultrasound machines, making it suitable for the large-scale industrial production of the ZnO/MoS_2/graphene heterostructure.

2. Materials and Methods

2.1. Preparation of Graphene Nanoplatelets

Graphene nanoplatelets were produced by dispersing expanded highly oriented pyrolytic graphite (HOPG; Aldrich product # 332461, Shanghai, China) in N-methyl-pyrrolidone (NMP; spectrophotometric 99.0%) solvent via bath sonication (100 kHz) for 10 h at 60 °C [36]. After that, the samples were centrifuged at 10,000 rpm for 1 h to extract the macroscopic aggregations. After repeating the sonication and centrifugation processes 3 times, a homogeneous gray solution was obtained. This liquid-phase exfoliation method was employed to obtain graphene solutions for various graphene concentrations (up to 2.5 mg ml^{-1}). In order to evaluate the morphology and quality of these samples, a small quantity of diluted graphene solution was dropped on the 300 nm SiO_2/Si wafer and dried for further characterizations by scanning electron microscopy (SEM) and Raman spectroscopy.

2.2. Preparation of MoS_2 Nanoplatelets

Similar to the preparation of graphene nanoplatelets, we prepared MoS_2 nanoplatelets by electrochemical-assisted liquid-phase exfoliation methods. First, we pretreated the MoS_2 crystals to be expanded to be bulk MoS_2 by using the electrochemical method previously reported by Duan's group [37]. The expanded MoS_2 crystal was sonicated in the dimethylformamide (DMF) solvent with the stabilizing-agent Poly-vinylpyrrolidone (PVP; molecular weight of about 40,000, Sigma-Aldrich, Shanghai, China), which effectively minimized the re-stacking of the MoS_2 nanoplatelets for 6 h to obtain the MoS_2 nanoplatelets. After the sonication and centrifugation processes were repeated, various concentrations (up to around 5 mg ml^{-1}) of MoS_2 solutions were produced. The solution exhibited a uniform yellow color due to the strong absorption of visible light by MoS_2. The SEM and Raman spectroscopy data were collected by dropping the MoS_2 nanoplatelets onto the surface of a 90 nm SiO_2/Si wafer.

2.3. Preparation of ZnO Nanoparticles

In the process of synthesizing ZnO nanoparticles, 22 mg of zinc acetate dihydrate ($Zn(CH_3COO)_2{\cdot}2H_2O$; 99.999%, Sigma-Aldrich, Shanghai, China) was refluxed and dissolved in 10 mL ethanol at 80 °C. A potassium hydroxide solution, prepared from 95 mg of potassium hydroxide (KOH; ≥ 85%, Sigma-Aldrich, Shanghai, China) sonicated in 10 ml ethanol, was slowly added dropwise to the zinc acetate solution in a water bath at 50 °C under magnetic stirring. The reaction conditions were maintained for 1 h, and the resulting transparent solution was kept overnight, extracted with n-hexane and ethanol, washed, and air-dried.

2.4. Assemblage of ZnO/MoS_2/Graphene Heterostructures

First, in order to assemble the MoS_2/graphene van der Waals heterostructures, dried MoS_2 and graphene nanoplatelets were mixed and added into deionized water for dispersion and gelatinization. After that, the mixture solution was centrifuged at 4000 rpm for 30 min and dried at 200 °C on the hot plate in order to obtain the MoS_2/graphene nanocomposites. It is worth noting that there may be existing a small amount of self-stacking graphene and MoS_2 nanoflakes in the composite. After the preparation of MoS_2/graphene heterostructures, we mixed prefabricated ZnO nanoparticles with dried MoS_2/graphene in 20 mL deionized water, using the magnetic stirrer (mass fraction: MoS_2 ~7 wt %; graphene ~3 wt %; and ZnO ~90 wt %), to ultimately produce the ZnO/MoS_2/graphene heterostructures shown in Figure 1.

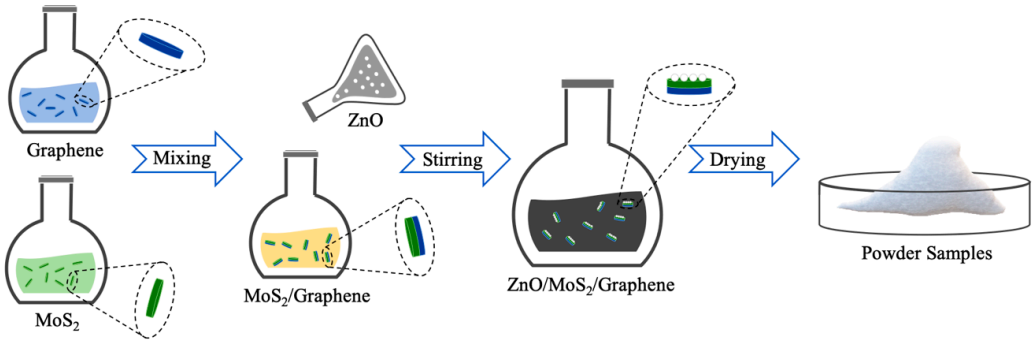

Figure 1. Schematics of manufacture processes of zinc oxide (ZnO)/molybdenum disulfide (MoS_2)/graphene heterostructures.

2.5. Characterization of Materials

Raman spectra and mappings of graphene and MoS_2 were obtained using confocal Raman spectroscopy (WITec Alpha 300R, Ulm, Germany) with a 488 nm laser wavelength, a 10 mW laser energy power, and a 300 nm resolution. The morphology of the nanomaterials was obtained by imaging

using a scanning electron microscope (SEM; ZEISS MERLIN, Jena, Germany). The components were detected by x-act with INCA and Aztec energy-dispersive X-ray spectroscopy (EDS) analysis software (Oxford Instruments, London, UK). The morphology and size of ZnO nanoparticles were measured by transmission electron microscope (TEM; Titan Themis Z, Oregon, USA) with an accelerating voltage of 300 kV. The X-ray diffraction patterns of the samples were tested using an X-ray diffractometer (XRD; Bruker D8 ADVANCE, Karlsruhe, Germany) with Cu (Kα) at a speed of 2°/min. The structures were detected by the X-ray photoelectron spectrometer (XPS; Kratos AXIS Ultra DLD, Manchester, UK). The UV-visible spectra of the samples were recorded on a spectrophotometer (Thermo Evolution 600 UV-Vis, Atlanta, OR, USA).

2.6. Evaluation of Photocatalytic Activity

Hydrogen-generation photocatalytic measurements were conducted in a homemade quartz reactor system. Photocatalysts were placed into the deionized water with sacrificial reagents of sodium sulfide (Na_2S; Sigma-Aldrich #407410) and sodium sulfite (Na_2SO_3; ≥ 85%, Sigma-Aldrich). The resulting mixture was stirred for 1 h without light in order to obtain a uniform dispersion. In the meantime, the nitrogen gas was introduced to exhaust the oxygen of the reaction chamber. We exposed the Xenon lamp (300 W, MKS 300XF, Kentucky, MA, USA), with a 400 nm center-wavelength standard bandpass filter, continuously stirred the reactor, and then measured the light intensities by the optical sensor. Meanwhile, the generated hydrogen was collected and analyzed using gas chromatography (Shimadzu, Nexis SCD-2030, Kyoto, Japan).

3. Results

3.1. Morphology Characterization of Materials

The SEM characterization of the morphology of prepared MoS_2 and graphene nanoplatelets are shown in Figure 2: Both of the prepared MoS_2 and graphene exhibited layered structures can be seen in Figure 2a,b. It is evident that the graphene nanoplatelets exhibited an approximately 10 um flake sizes, while the MoS_2 nanosheets displayed a flake size of approximately 1 um. Meanwhile, Figure 2c shows a uniform distribution of ZnO nanoparticles. From the SEM image in Figure 2d, we can clearly see that the smaller-sized MoS_2 nanoplatelets tended to adhere to the surface of larger-sized graphene nanoplatelets to form the heterostructures due to the van der Waals effect. In addition, the heterostructure of ZnO/MoS_2 can be observed in Figure 2e, in which a large amount of ZnO nanocrystals is distributed on the surface of the MoS_2. Similarly, the final heterostructures of the ZnO/MoS_2/graphene ternary composite are shown in Figure 2f, with the uniformly distributed ZnO nanoparticles on the interlayered MoS_2 and bottom-layered graphene nanoplatelets. To further confirm the existence of every element component, the energy-dispersive X-ray spectroscopy (EDS) was conducted on the samples of the MoS_2/graphene heterostructure, the ZnO/MoS_2 heterostructure, and the ZnO/MoS_2/graphene ternary heterostructure, respectively. The typical element components of each material were measured, which further confirmed the formation and existence of these heterostructures, as shown in Figure 2g,h,i.

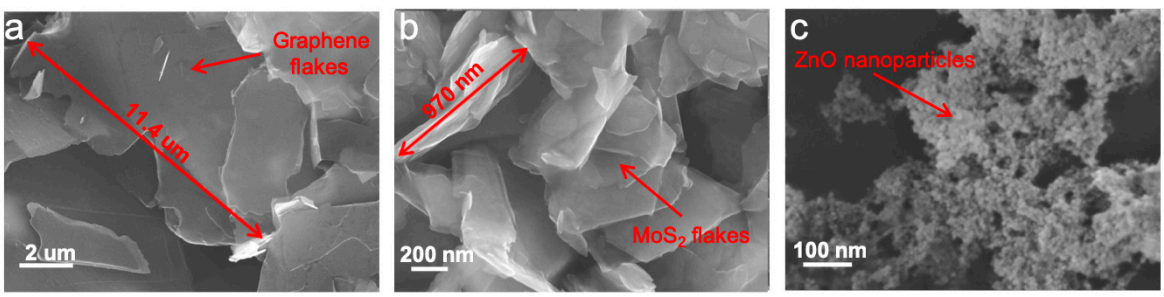

Figure 2. *Cont.*

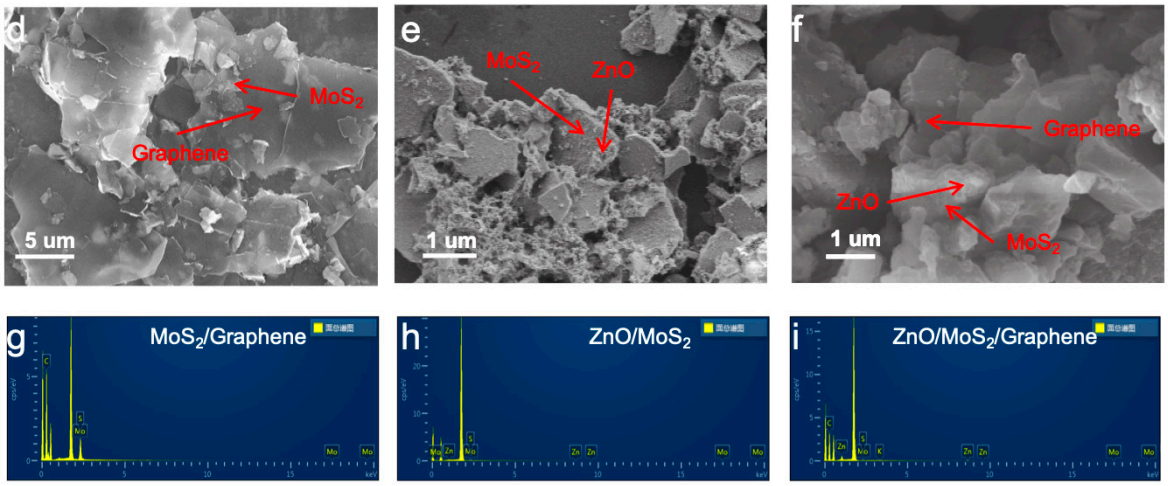

Figure 2. Morphology characteristics of the different samples. (**a**) SEM images of graphene nanoplatelets; (**b**) SEM images of MoS_2 nanoplatelets; (**c**) SEM images of ZnO nanoparticles; (**d**) SEM images of MoS_2/graphene; (**e**) SEM images of ZnO/MoS_2, (**f**) SEM images of ZnO/MoS_2/graphene; (**g**) energy-dispersive X-ray spectroscopy (EDS) of MoS_2/graphene heterostructures; (**h**) EDS of ZnO/MoS_2 heterostructures; (**i**) EDS of ZnO/MoS_2/graphene ternary heterostructures.

3.2. *Structural Characterization of Materials*

The structural analysis of the various items and their components was performed using XRD, XPS, Raman, and PL spectroscopy. Figure 3a shows the XRD images of ZnO, graphene, MoS_2, and the ZnO/MoS_2/graphene ternary heterostructures. For pure ZnO nanocrystals, the diffraction peaks appeared at 2θ = 31.3, 34.6, 36.1, 47.7, 56.2, 62.9, and 67.7; these peaks can be attributed to (100), (002), (101), (102), (110), (103), and (112) lattice planes, respectively. A comparison of the XRD patterns with the (100), (002), (101) and other diffraction peaks of standard ZnO materials demonstrates the existence of a polycrystalline hexagonal wurtzite crystal orientation for ZnO [38]. When we compared the XRD data of pure ZnO with ZnO/MoS_2/graphene, it was easy to see that the (100), (002), and (101) diffraction peaks had a slight left shift, indicating that the ZnO lattice constant became larger due to the strong interactions of van der Waals forces in the heterostructures. Moreover, with respect to the pure MoS_2 nanosheets, we compared the diffraction peak positions with the standard card JCPDS 37-1492, which was consistent with our results, proving that the product is a hexagonal phase. Moreover, the presence of the (002) peak indicated a good crystallization of the sample. The XRD diffraction spectrum of graphene nanoplatelets exhibited a standard graphene diffraction peak at 2θ = 26°, which was different from the diffraction peak of graphene oxide at 2θ = 10°. This indicates that there are no damages or defects between the layers of graphene, as proof of its excellence. Regarding the ZnO/MoS_2/graphene heterostructures, they mainly exhibited the diffraction peak characteristic of ZnO, owing to the fewer components of graphene and MoS_2 in the composition.

Further, XPS spectra are shown in Figure 3b, the C-1s peak of 284.3 eV mainly corresponded to the C-C of sp^2 hybridization in graphene [39]. Furthermore, the peaks observed at 1020 eV and 1045 eV corresponded to the $2p^{3/2}$ and $2p^{1/2}$ peaks of Zn-2p, respectively, which was assigned to the ZnO [40]. We can find that, in pure ZnO, the two peaks of $2p^{3/2}$ and $2p^{1/2}$ of Zn-2p had a very slight shift. The reason may be that the formation of a heterojunction in the complex that promoted the charge transferring. In addition, we also observed Mo-3d and S-2p core levels at 228.4 eV and 162.1 eV in agreement to previous reports [41–44]. The High Resolution-XPS results of C-1s, Mo-3d, and S-2p are shown in the Supporting Information (Figure S1, Supporting Information). From the HR-XPS data of Mo-3d core level, we can conclude that there is only a Mo^{4+} chemical state corresponding to MoS_2. Moreover, considering that the MoS_2 is prepared by a physical method (electro-assisted liquid-phase exfoliation method), almost no MoO_x exists in the composite, resulting in the lack of another doublet peak of Mo-3d in the XPS result.

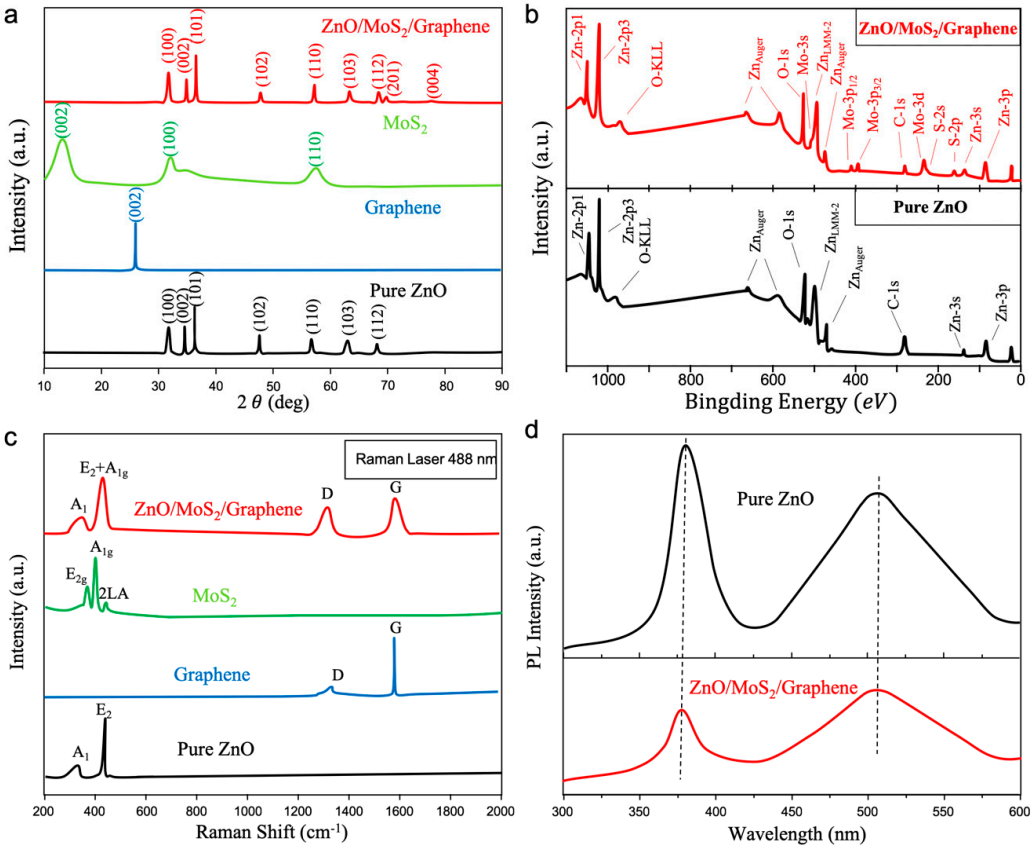

Figure 3. Structural characterization of the various samples. (**a**) XRD measurements of each component; (**b**) X-ray photoelectron spectrometer (XPS) data of pure ZnO and ZnO/MoS_2/graphene heterostructures; (**c**) Raman characterizations of each component; (**d**) photoluminescence (PL) spectra of the ZnO and ZnO/MoS_2/graphene heterostructures.

To further characterize the quality of materials, the Raman spectra of ZnO, graphene, MoS_2, and ZnO/MoS_2/graphene were measured, as shown in Figure 3c, which illustrated the small defect peak of prepared graphene nanoflakes as the superior electron-accepting layers, and the physical prepared multi-layered MoS_2 nanosheets as the excellent electron-transport-layered materials. However, after combining the graphene nanosheets with other materials to form the heterostructures, the D peak of the graphene in the composite became significantly higher, due to the influence of the internal effect in the heterojunction. Simultaneously, this effect was also found in the ZnO, which is evidenced by the left shift of the ZnO diffraction peaks in the XRD spectra. An explanation for this is that an increase of the lattice constant causes the occurrence of more oxygen-vacancy defects, which further results in an increase of the visible-light absorption capacity of the materials, eventually improving the catalytic efficiency of the composite. In addition, from the Raman spectra of ZnO/MoS_2/graphene composite, we are able to explain the widening A1 and E2 peaks by the superimposition of the Raman signals from MoS_2 and pure ZnO nanoparticles.

Photoluminescence (PL) spectra were also measured on the ZnO nanoparticles and ZnO/MoS_2/graphene heterostructures at room temperature, as given in Figure 2d, for an excitation wavelength of the PL spectrum of 372 nm. It is evident from the PL spectrum that by combining ZnO with MoS_2/graphene, the PL emission peak was reduced, indicating less photogenerated electron-hole recombination. The mechanism can be described as follows: The photogenerated electrons are more naturally diffuse into the graphene layer due to the excellent carrier mobility of graphene and the matched energy levels ($E_c^{ZnO} > E_c^{MoS_2} > E_{Fermi}^{graphene}$), resulting in an extension of the excited-carrier lifetime. Taking into account the fact that the existences of ZnO and MoS_2 increases the specific surface area, the adsorption capacity of the ZnO/MoS_2/graphene was enhanced and led to a high photocatalytic ability.

3.3. Micromechanism of Enhanced Photocatalytic Effects

The designed ZnO/MoS_2/graphene heterostructures and the electron transfer during the photocatalytic processes are illustrated in Figure 4. The primary reasons for the excellent photocatalytic ability of ZnO/MoS_2/graphene can be summarized as follows: (1) Introducing a MoS_2 layer increases the specific surface area and inhibits the self-stacking of graphene nanoplatelets, providing more active sites [45–48]. (2) The energy levels of MoS_2 and graphene are reasonably matched, enhancing the electron transportation between layered materials; in this way, the possibilities of photogenerated electron-hole recombination are lowered. (3) As a two-dimensional material with higher carrier mobilities, graphene acts as an excellent electron acceptor. (4) The interlayer MoS_2 serves as a visible-light absorbance material in this structure due to its adequate band gap. The band gaps of multi-layer MoS_2 nanoplatelets and ZnO nanocrystals are 1.29 eV and 3.29 eV, respectively [49]. According to the previous report, we know that the values of E_c^{Zno} and $E_c^{MoS_2}$ are −0.31 and −0.11 eV, respectively [14]. Considering the fact that $E_c^{ZnO} > E_c^{MoS_2} > E_{Fermi}^{graphene}$, the photogenerated electrons in ZnO are easily transferred to the graphene nanoplatelets through MoS_2, as shown in Figure 4b. Moreover, due to the existence of interlayered MoS_2, electrons can travel faster, which reduces the possibility of the recombination of electrons and holes [50,51]. Lastly, the electron-storage capacity of pure graphene nanoplatelets is superior to that of reduced graphene oxide or graphene oxide, because the nanoplatelets do not bond with any functional group, resulting in a higher photocatalytic ability.

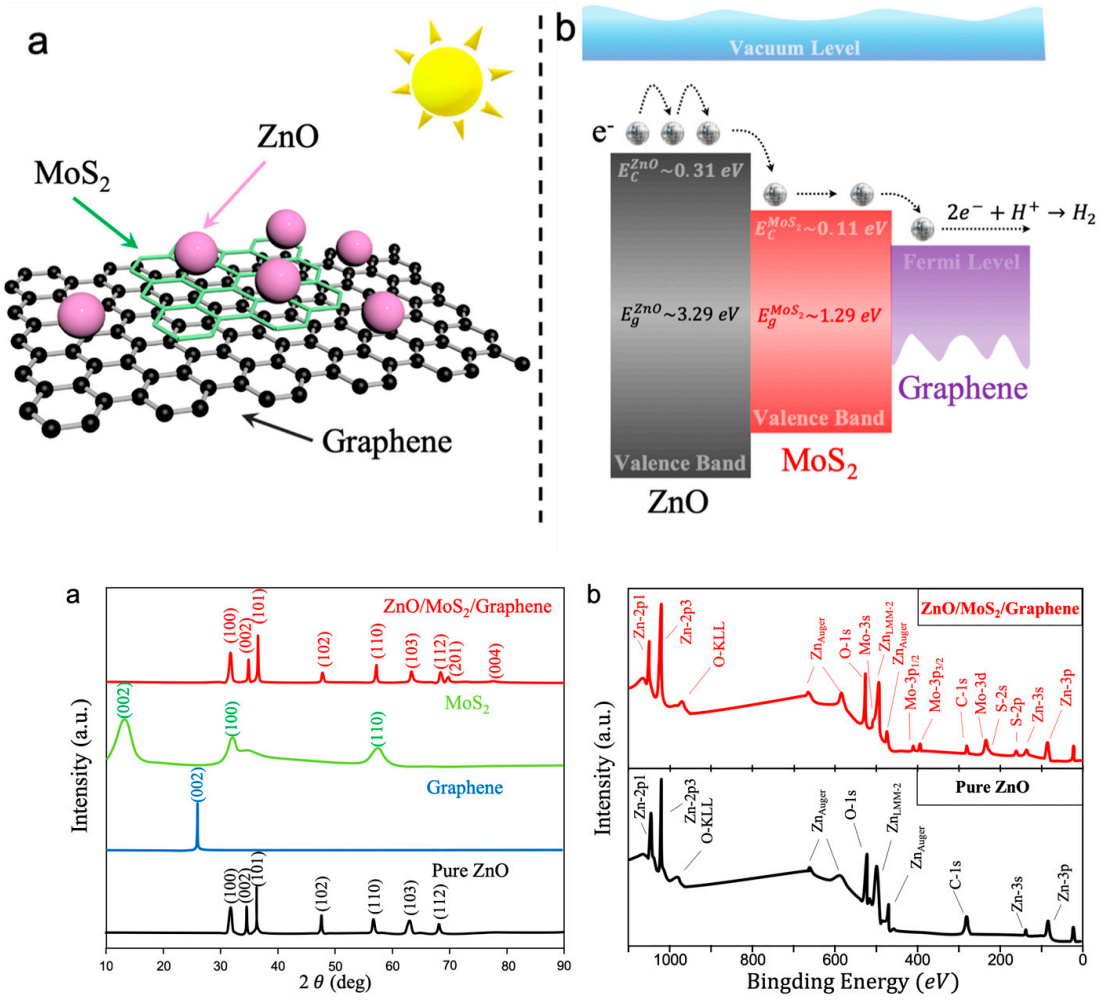

Figure 4. *Cont.*

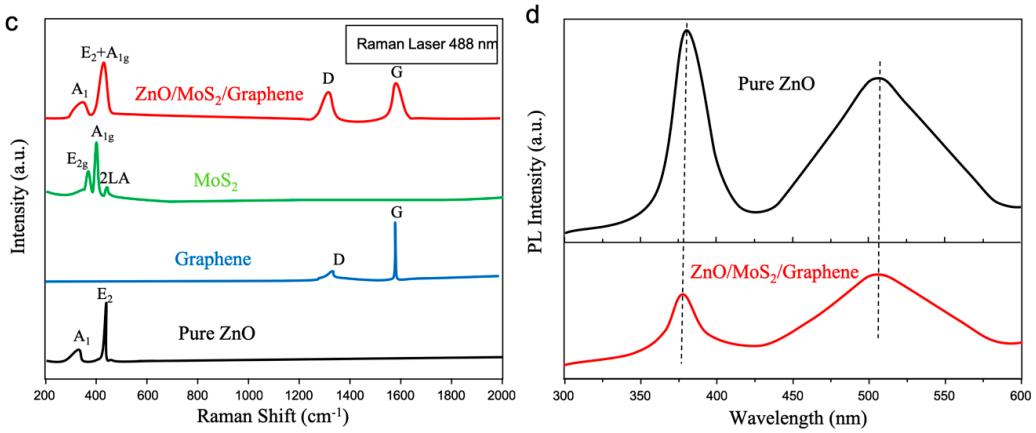

Figure 4. Schematics of heterostructures and electron transfer in photocatalytic processes. (**a**) 3D view of the ZnO/MoS_2/graphene heterostructures; (**b**) energy diagram and generated electrons transfer during visible-light illumination.

3.4. Photocatalytic Measurements

The photocatalytic activity was evaluated by measuring the ability of hydrogen generation under visible-light illumination in various photocatalysts. Figure 5a compares the results of the photocatalytic abilities of four nanomaterials, ZnO, ZnO/graphene, ZnO/MoS_2, and ZnO/MoS_2/graphene. The hydrogen generation rate is nearly zero with the ZnO photocatalyst only, whereas ZnO/MoS_2/graphene leads to maximum hydrogen generation. Due to the synergistic effect of MoS_2 and graphene nanoplatelets, the recombination rate of photogenerated electron-hole pairs is strongly reduced. Figure 5b shows the differences between these five types of components regarding photocatalytic efficiency. From this diagram we know that the maximum efficiency is achieved with ~ 90% ZnO, ~ 7% MoS_2, and ~ 3% graphene. This phenomenon can be explained by the various roles played by ZnO, MoS_2, and graphene in the catalytic process. A sufficient amount of ZnO nanoparticles provided a large number of photogenerated electrons, leading to an increase of the hydrogen generation rates of the photocatalysts [52–54]. We also notice that the self-limiting effect exists in the photocatalytic process because the catalyst itself hinders the catalytic reaction.

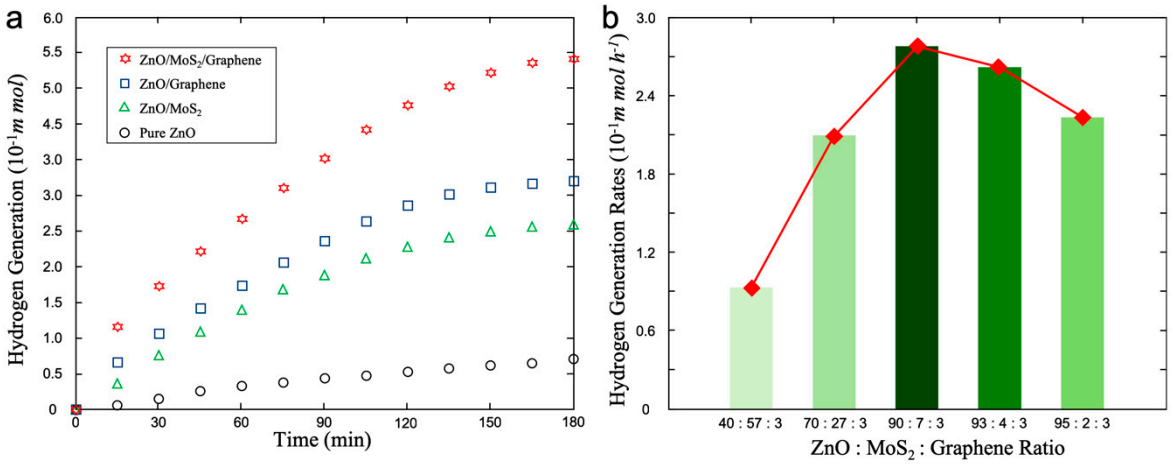

Figure 5. Photocatalytic efficiency measurements. (**a**) Diagram of hydrogen generation rates of ZnO, ZnO/graphene, ZnO/MoS_2, and ZnO/MoS_2/graphene catalysts; (**b**) hydrogen generation rates diagram of various componential ZnO/MoS_2/graphene photocatalysts.

In comparison with separate studies referenced in this paper, the ZnO/MoS_2 photocatalyst prepared by Yuan et al. has a catalytic efficiency of about 0.8 mmol h^{-1} g^{-1} [46]; they also prepared a MoS_2-graphene/$ZnIn_2S_4$ composite with a catalytic efficiency of about 4.2 mmol h^{-1} g^{-1} [49].

Bhirud et al. prepared N–ZnO/graphene nanocomposites, whose catalytic efficiency reached about 5 mmol h^{-1} g^{-1} [55]. Kumar et al. prepared a ZnO–MoS_2–Reduced Graphene Oxide composite with a catalytic efficiency of 28.6 mmol h^{-1} g^{-1} [14]. In this work, we prepared a ZnO/MoS_2/graphene composite, whose catalytic efficiency can reach 5.4 mmol h^{-1} g^{-1} (we measured 50 mg photocatalyst and converted to the same units). As a comparison, we can conclude that this work provides a high-throughput method for preparing higher-efficiency photocatalytic materials, which has a driving role in the application of photocatalysis in industry.

4. Conclusions

In this study, we presented a novel high-efficient photocatalyst based on the ZnO/MoS_2/graphene sandwiched heterostructures. This new material was synthesized by taking advantage of the high electron densities of ZnO nanoparticles, the ultra-high electron mobilities and specific surface area of graphene nanoplatelets, and the enhanced visible-light absorption properties of MoS_2, which allowed a highly efficient production of hydrogen by ZnO/MoS_2/graphene enabled photocatalysis. Also, the production of these materials occurred mainly through chemical and liquid-phase exfoliations, which are suitable for large-scale industrial production. In summary, this work combined the excellent properties of zero-dimensional nanoparticles and two-dimensional nanomaterials, developed a novel layer-by-layer nanostructured photocatalyst, and eventually realized a highly efficient hydrogen production under sunlight. It opens new avenues for the high-throughput production of superior hydrogen-evolution photocatalysts that are of significant importance to a clean energy revolution.

Supplementary Materials: The following are available online at http://www.mdpi.com/1996-1944/12/14/2233/s1. Figure S1. HR XPS of C-1s, Mo-3d and S-2p after reducing noisy.

Author Contributions: H.D., Y.X., B.T., and X.Z. conceived and directed this work. J.L. and M.C. fabricated the materials of graphene and MoS_2. H.W. and X.J. conducted Raman and SEM characterizations. H.D., B.T., and X.Z. analyzed all data and wrote the paper with contribution from all co-authors.

Funding: This research received no external funding.

Acknowledgments: This work was supported by funding from King Abdullah University of Science and Technology (KAUST), under award number: URF/1/2634 (CRG4) and URF/1/2996 (CRG5). This work was also supported by the National Natural Science Foundation of China (11835008 and 51872250), the State Key Laboratory of Intense Pulsed Radiation Simulation and Effect (Northwest Institute of Nuclear Technology, SKLIPR1814) and Low Dimensional Materials &Application Technology of Ministry of Education (Xiangtan University, KF20180203).

Conflicts of Interest: The authors declare no conflicts of interest

References

1. Roldán, M.L.; Corrad, G.; Francioso, O.; Sanchez-Cortes, S. Interaction of soil humic acids with herbicide paraquat analyzed by surface-enhanced Raman scattering and fluorescence spectroscopy on silver plasmonic nanoparticles. *Anal. Chim. Acta* **2011**, *699*, 87–95. [CrossRef] [PubMed]
2. Xiang, Q.; Yu, J.; Jaroniec, M. Adsorptive remediation of environmental pollutants using novel graphene-based nanomaterials. *Chem. Eng. J.* **2013**, *226*, 336–347.
3. Neena, D.; Kiran, K.K.; Han, B.; Dingze, L.; Pravin, K.; Dwivedi, R.K.; Vasiliy, O.P.; Zhao, X.; Gao, W.; Fu, D. Enhanced visible light photodegradation activity of RhB/MB from aqueous solution using nanosized novel Fe-Cd co-modified ZnO. *Sci. Rep.* **2018**, *8*, 10691.
4. Kansal, S.K.; Singh, M.; Sud, D. Studies on photodegradation of two commercial dyes in aqueous phase using different photocatalysts. *J. Hazard. Mater.* **2007**, *141*, 581–590. [CrossRef] [PubMed]
5. Gholami, M.; Shirzad-Siboni, M.; Farzadkia, M.; Yang, J.K. Synthesis, characterization, and application of ZnO/TiO2 nanocomposite for photocatalysis of a herbicide (Bentazon). Desalin. *Water Treat.* **2016**, *57*, 13632–13644. [CrossRef]
6. Zhang, X.; Xiang, J.; Mu, C.; Wen, F.; Yuan, S.; Zhao, J.; Dong, Y.X.; Can, S.; Zhong, Y.L. SnS2 Nanoflakes Anchored Graphene obtained by Liquid Phase Exfoliation and MoS_2 Nanosheet Composites as Lithium and Sodium Battery Anodes. *Electrochim. Acta* **2017**, *227*, 203–209. [CrossRef]

7. Kalyani, D.; McMurtrey, K.B.; Neufeldt, S.R.; Sanford, M.S. Room-temperature C-H arylation: Merger of Pd-catalyzed C-H functionalization and visible-light photocatalysis. *J. Am. Chem. Soc.* **2012**, *143*, 16516–16519. [CrossRef]
8. Rahimi, K.; Yazdani, A.; Ahmadirad, M. Facile preparation of zinc oxide nanorods surrounded by graphene quantum dots both synthesized via separate pyrolysis procedures for photocatalyst application. *Mater. Res. Bull.* **2018**, *98*, 148–154. [CrossRef]
9. Chang, C.M.; Hon, M.H.; Leu, I.C. Outstanding H2 sensing performance of Pd nanoparticle-decorated ZnO nanorod arrays and the temperature-dependent sensing mechanisms. *ACS Appl. Mater. Interfaces* **2013**, *5*, 135–143. [CrossRef]
10. Xie, G.; Zhang, K.; Guo, B.; Liu, Q.; Fang, L.; Gong, J.R. Graphene-based materials for hydrogen generation from light-driven water splitting. *Adv. Mater.* **2013**, *25*, 3820–3839. [CrossRef]
11. Punithavathy, I.K.; Richard, J.P.; Jeyakumar, S.J.; Jothibas, M.; Praveen, P. Photodegradation of methyl violet dye using ZnO nanorods. *J. Mater. Sci. Mater. Electron.* **2017**, *28*, 2494–2501. [CrossRef]
12. Huang, K.; Li, Y.H.; Lin, S.; Liang, C.; Wang, H.; Ye, C.X.; Wang, Y.G.; Zhang, R.; Fan, D.Y.; Yang, H.J. A facile route to reduced graphene oxide–zinc oxide nanorod composites with enhanced photocatalytic activity. *Powder Technol.* **2014**, *257*, 113–119. [CrossRef]
13. Moussa, H.; Girot, E.; Mozet, K.; Alem, H.; Medjahdi, G.; Schneider, R. ZnO rods/reduced graphene oxide composites prepared via a solvothermal reaction for efficient sunlight-driven photocatalysis. *Appl. Catal. B Environ.* **2016**, *185*, 11–21. [CrossRef]
14. Suneel, K.; Nagappagari, L.R.; Himmat, S.K.; Ashish, K.; Muthukonda, V.S.; Kaustava, B.; Aditi, H.; Venkata, K. Efficient Electron Transfer across a ZnO-MoS_2-Reduced Graphene Oxide Heterojunction for Enhanced Sunlight-Driven Photocatalytic Hydrogen Evolution. *Chemsuschem* **2017**, *10*, 3588–3603.
15. Novoselov, K.S.; Geim, A.K.; Morozov, S.V.; Jiang, D.; Katsnelson, M.I.; Grigorieva, I.V.; Dubonos, S.V.; Firsov, A.A. Two-dimensional gas of massless Dirac fermions in graphene. *Nature* **2005**, *438*, 197–200. [CrossRef]
16. Qin, H.; Li, W.; Xia, Y.; He, T. Photocatalytic Activity of Heterostructures Based on ZnO and N-Doped ZnO. *Acs Appl. Mater. Interfaces* **2011**, *3*, 3152–3156. [CrossRef]
17. Lonkar, S.P.; Pillai, V.V.; Alhassan, S.M. Three-Dimensional NiS-MoS_2/Graphene Heterostructured Nanohybrids as High-Performance Hydrodesulfurization Catalysts. *ACS Appl. Nano Mater.* **2018**, *1*, 3114–3123. [CrossRef]
18. Nguyen, D.C.T.; Cho, K.Y.; Oh, W.C. Synthesis of frost-like CuO combined graphene-TiO2 by self-assembly method and its high photocatalytic performance. *Appl. Surf. Sci.* **2017**, *412*, 252–261. [CrossRef]
19. Liu, H.; Liu, S.; Zhang, Z. Hydrothermal etching fabrication of TiO2 at graphene hollow structures mutually independent exposed {001} and {101} facets nanocrystals and its synergistic photocaltalytic effects. *Sci. Rep.* **2016**, *6*, 33839. [CrossRef]
20. Dong, Y.; Shao, J.; Chen, C.; Li, H.; Wang, R.; Chi, Y.; Lin, X.; Chen, G. Blue luminescent graphene quantum dots and graphene oxide prepared by tuning the carbonization degree of citric acid. *Carbon* **2012**, *50*, 4738–4743. [CrossRef]
21. Hamad, A.F.; Alkureishi, L.W.T.; Shoaib, T. Reminder of important clinical lesson: Sentinel node biopsy in floor of mouth cancers: The need to clear level I. *BMJ Case Rep.* **2009**, bcr0920081015.
22. Zhang, Q.; Bao, N.; Wang, X.; Hu, X.; Miao, X.; Chaker, M.; Ma, D. Advanced Fabrication of Chemically Bonded Graphene/TiO2 Continuous Fibers with Enhanced Broadband Photocatalytic Properties and Involved Mechanisms Exploration. *Sci. Rep.* **2016**, *6*, 38066. [CrossRef] [PubMed]
23. Chen, D.; Li, S.; Xu, B.; Zheng, F.; Zhou, H.; Yu, H.; Lin, F.; Zhu, X. Polycrystalline iron oxide nanoparticles prepared by C-dot-mediated aggregation and reduction for supercapacitor application. *RSC Adv.* **2016**, *6*, 45023–45030. [CrossRef]
24. Chang, K.; Mei, Z.; Wang, T.; Kang, Q.; Ouyang, S.; Ye, J. MoS_2/graphene cocatalyst for efficient photocatalytic H2 evolution under visible light irradiation. *ACS Nano* **2014**, *8*, 7078–7087. [CrossRef] [PubMed]
25. Li, Y.; Wang, H.; Xie, L.; Liang, Y.; Hong, G.; Dai, H. MoS_2 nanoparticles grown on graphene: an advanced catalyst for the hydrogen evolution reaction. *J. Am. Chem. Soc.* **2011**, *133*, 7296–7299. [CrossRef] [PubMed]
26. Wang, H.; Lee, H.W.; Deng, Y.; Lu, Z.; Hsu, P.C.; Liu, Y.; Lin, D.; Cui, Y. Bifunctional non-noble metal oxide nanoparticle electrocatalysts through lithium-induced conversion for overall water splitting. *Nat. Commun.* **2015**, *6*, 7261. [CrossRef] [PubMed]

27. Chen, C.; Mei, W.; Yu, W.; Chen, X.A.; Zeng, L.; Tsang, Y.; Chao, Z.; Liu, X. Enhanced sunlight-driven photocatalytic property of Mg-doped ZnO nanocomposites with three-dimensional graphene oxide/MoS_2 nanosheet composites. *RSC advances.* **2018**, *8*, 17399–17409. [CrossRef]
28. Ha, E.; Liu, W.; Wang, L.; Man, H.W.; Hu, L.; Tsang, S.C.E.; Chan, C.T.L.; Kwok, W.; Lee, L.Y.S.; Wong, K.Y. Cu2ZnSnS4/MoS_2-Reduced Graphene Oxide Heterostructure: Nanoscale Interfacial Contact and Enhanced Photocatalytic Hydrogen Generation. *Sci. Rep.* **2017**, *7*, 39411. [CrossRef]
29. Nguyen, E.P.; Carey, B.J.; Daeneke, T.; Ou, J.Z.; Latham, K.; Zhuiykov, S.; Kalantar-zadeh, K. Investigation of two-solvent grinding-assisted liquid phase exfoliation of layered MoS_2. *Chem. Mater.* **2014**, *27*(1), 53–59. [CrossRef]
30. Islam, S.E.; Hang, D.R.; Chen, C.H.; Sharma, K.H. Facile and Cost-efficient Synthesis of Quasi 0D/2D ZnO/MoS_2 Nanocomposites for Highly Enhanced Visible-light-driven Photocatalytic Degradation of Organic Pollutants and Antibiotic. *Chemistry* **2018**, *24*, 9305–9315. [CrossRef]
31. Chang, K.; Chen, W. In Situ synthesis of MoS_2/graphene nanosheet composites with extraordinarily high electrochemical performance for lithium ion batteries. *Chem. Commun.* **2011**, *47*, 4252–4254. [CrossRef] [PubMed]
32. Kwak, J.Y.; Hwang, J.; Calderon, B.; Alsalman, H.; Munoz, N.; Schutter, B.; Spencer, M.G. Electrical characteristics of multilayer MoS_2 FET's with MoS_2/graphene heterojunction contacts. *Nano Lett.* **2014**, *14*, 4511–4516. [CrossRef] [PubMed]
33. Xia, S.; Wang, Y.; Liu, Y.; Wu, C.; Wu, M.; Zhang, H. Ultrathin MoS_2 nanosheets tightly anchoring onto nitrogen-doped graphene for enhanced lithium storage properties. *Chem. Eng. J.* **2018**, *332*, 431–439. [CrossRef]
34. Pan, F.; Ding, H.; Li, W.; Song, Y.; Yang, H.; Wu, H.; Jiang, Z.; Wang, B.; Cao, X. Constructing facilitated transport pathway in hybrid membranes by incorporating MoS_2 nanosheets. *J. Membr. Sci.* **2018**, *545*, 29–37. [CrossRef]
35. Liu, W.W.; Xia, B.Y.; Wang, X.X.; Wang, J.N. Exfoliation and dispersion of graphene in ethanol-water mixtures. *Front. Mater. Sci.* **2012**, *6*, 176–182. [CrossRef]
36. Tian, B.; Lin, W.; Zhuang, P.; Li, J.; Shih, T.M.; Cai, W. Magnetically-induced alignment of graphene via Landau diamagnetism. *Carbon* **2018**, *131*, 66–71. [CrossRef]
37. Lin, Z.; Liu, Y.; Halim, U.; Ding, M.; Liu, Y.; Wang, Y.; Jia, C.; Chen, P.; Duan, X.; Wang, C.; et al. Solution-processable 2D semiconductors for high-performance large-area electronics. *Nature* **2018**, *562*, 254–258. [CrossRef] [PubMed]
38. Wu, T.; Wang, Z.; Tian, M.; Miao, J.; Zhang, H.; Sun, J. UV excitation NO2 gas sensor sensitized by ZnO quantum dots at room temperature. *Sens. Actuat. B: Chem.* **2018**, *259*, 526–531. [CrossRef]
39. Chu, J.; Han, X.; Yu, Z.; Du, Y.; Song, B.; Xu, P. Highly efficient visible-light-driven photocatalytic hydrogen production of CdS-cluster-decorated graphene nanosheets. *J. Am. Chem. Soc.* **2011**, *133*, 10878–10884.
40. Samadi, M.; Shivaee, H.A.; Zanetti, M.; Pourjavadi, A.; Moshfegh, A. Visible light photocatalytic activity of novel MWCNT-doped ZnO electrospun nanofibers. *J. Mol. Catal. A Chem.* **2012**, *359*, 42–48. [CrossRef]
41. Ganta, D.; Sinha, S.; Haasch, R.T. 2-D material molybdenum disulfide analyzed by XPS. *Surf. Sci. Spectra* **2014**, *21*, 19–27. [CrossRef]
42. Addou, R.; McDonnell, S.; Barrera, D.; Guo, Z.; Azcatl, A.; Wang, J.; Zhu, H.; Hinkle, C.L.; Quevedo-Lopez, M.; Alshareef, H.N.; et al. Impurities and electronic property variations of natural MoS_2 crystal surfaces. *ACS Nano* **2015**, *9*, 9124–9133. [CrossRef] [PubMed]
43. McDonnell, S.; Azcatl, A.; Addou, R.; Gong, C.; Battaglia, C.; Chuang, S.; Cho, K.; Javey, A.; Wallace, R.M. Hole contacts on transition metal dichalcogenides: Interface chemistry and band alignments. *ACS Nano* **2014**, *8*, 6265–6272. [CrossRef] [PubMed]
44. Diaz, H.C.; Addou, R.; Batzill, M. Interface properties of CVD grown graphene transferred onto MoS_2 (0001). *Nanoscale* **2014**, *6*, 1071–1078. [CrossRef]
45. Kumar, S.; Sharma, V.; Bhattacharyya, K.; Krishnan, V. N-doped ZnO–MoS_2 binary heterojunctions: The dual role of 2D MoS_2 in the enhancement of photostability and photocatalytic activity under visible light irradiation for tetracycline degradation. *Mater. Chem. Front.* **2017**, *1*, 1093–1106. [CrossRef]
46. Long, L.L.; Chen, J.J.; Zhang, X.; Zhang, A.Y.; Huang, Y.X.; Rong, Q.; Yu, H.Q. Layer-controlled growth of MoS_2 on self-assembled flower-like Bi2S3 for enhanced photocatalysis under visible light irradiation. *NPG Asia Mater.* **2016**, *8*, e263. [CrossRef]

47. Sake, W.; Hongyu, T.; Chongdan, R.; Jin, Y.; Minglei, S. Electronic and optical properties of heterostructures based on transition metal dichalcogenides and graphene-like zinc oxide. *Sci. Rep.* **2018**, *8*, 12009.
48. Mishra, A.K.; Lakshmi, K.V.; Huang, L. Eco-friendly synthesis of metal dichalcogenides nanosheets and their environmental remediation potential driven by visible light. *Sci. Rep.* **2015**, *5*, 15718. [CrossRef]
49. Yuan, Y.J.; Wang, F.; Hu, B.; Lu, H.W.; Yu, Z.T.; Zou, Z.G. Significant enhancement in photocatalytic hydrogen evolution from water using a MoS_2 nanosheet-coated ZnO heterostructure photocatalyst. *Dalton Trans.* **2015**, *44*, 10997–11003. [CrossRef]
50. Ahmed, A.; Al-Amin, A.Q.; Ambrose, A.F.; Saidur, R. Hydrogen fuel and transport system: A sustainable and environmental future. *Int. J. Hydrog. Energy* **2016**, *41*, 1369–1380. [CrossRef]
51. Yuan, Y.J.; Tu, J.R.; Ye, Z.J.; Chen, D.Q.; Hu, B.; Huang, Y.W.; Chen, T.T.; Cao, D.; Yu, Z.; Zou, Z.G. MoS_2-graphene/ZnIn2S4 hierarchical microarchitectures with an electron transport bridge between light-harvesting semicondu ctor and cocatalyst: A highly efficient photocatalyst for solar hydrogen generation. *Appl. Catal. B Environ.* **2016**, *188*, 13–22. [CrossRef]
52. Xiang, Q.; Yu, J.; Jaroniec, M. Graphene-based semiconductor photocatalysts. *Chem. Soc. Rev.* **2012**, *41*, 782–796. [CrossRef] [PubMed]
53. Wang, M.; Ju, P.; Li, J.; Zhao, Y.; Han, X.; Hao, Z. Facile Synthesis of MoS_2/g-C3N4/GO Ternary Heterojunction with Enhanced Photocatalytic Activity for Water Splitting. *ACS Sustain. Chem. Eng.* **2017**, *5*, 7878–7886. [CrossRef]
54. Wu, J.; Xiao, D.; Wu, W.; Zhu, J.; Wang, J. Effect of dwell time during sintering on piezoelectric properties of (Ba0.85Ca0.15)(Ti0.90Zr0.10)O3 lead-free ceramics. *J. Alloy. Compd.* **2011**, *509*, 359–361. [CrossRef]
55. Bhirud, A.; Sathaye, S.; Waichal, R.; Park, C.J.; Kale, B. In situ preparation of N–ZnO/graphene nanocomposites: Excellent candidate as a photocatalyst for enhanced solar hydrogen generation and high performance supercapacitor electrode. *J. Mater. Chem. A* **2015**, *3*, 17050–17063. [CrossRef]

© 2019 by the authors. Licensee MDPI, Basel, Switzerland. This article is an open access article distributed under the terms and conditions of the Creative Commons Attribution (CC BY) license (http://creativecommons.org/licenses/by/4.0/).